Metals and Materials International (2020) 26:591–602
https://doi.org/10.1007/s12540-019-00360-w

Development and Microstructural Characterization of a New Wrought High Entropy Superalloy

Ahad Shafiee[1] · Mahmoud Nili-Ahmadabadi[1] · Hyoung Seop Kim[2] · Mohammad Jahazi[3]

Received: 14 March 2019 / Accepted: 4 July 2019 / Published online: 23 July 2019

Abstract
In this study, a newly developed γ′ precipitation hardened high entropy superalloy (designated as HES-A1 hereafter) was produced and its microstructural features were characterized. The new alloy composition is based on the major elements of conventional IN718 alloy, however other elements were added or removed to minimize possible presence of δ (or γ″) phase and increase the volume fraction of very fine γ′ precipitates instead. Broadening the hot working window, lower density, and avoiding the use of expensive elements were other considerations taken into account in the design of the new alloy. CALPHAD (CALculation of PHAse Diagrams) and PhaComp methods were used for the prediction of phases and their evolutions. The microstructure of the HES-A1 alloy in as-cast, homogenized, hot rolled, annealed and aged conditions were characterized using optical, scanning, and transmission electron microscopes as well as X-ray diffraction technique. The as-cast microstructure of HES-A1 contained 5.5% of Laves phase, which was reduced to less than 0.3% through the development of a homogenization treatment. Hot rolling with reductions up to 36% at 1015 °C did not produce any cracking, indicating a good forming potential for the new alloy. The application of double aging treatment, similar to the one for IN718 alloy, showed no presence of γ″ or formation of δ phase in the microstructure. HES-A1 has been designed with a higher Al/(Ti + Nb) ratio and higher proportion of Al + Ti + Nb so that it could be mainly strengthened by γ′ precipitation. The average size of monomodal γ′ precipitates was smaller than that observed in conventional alloys after similar treatments.

Keywords High entropy alloys · Superalloys · Alloy design · Casting · Heat treatment · Microstructure · Electron microscopy

1 Introduction

Superalloys, either cast or wrought, are generally used at temperatures above 540 °C [1]. Among wrought superalloys used for turbine disc applications, IN718 is the most widely used due to a suitable combination of high strength, good formability, lower density, and moderate cost [2–5]. However, the maximum service temperature of IN718 is about 649 °C, thereby, limiting its application in hotter sections of the turbine. This limitation has been mostly related to the presence of the γ″ strengthening phase and its transformation to δ over time [5]. As a result, extensive research has been undertaken to develop new alloys with higher service temperatures than IN718. Specifically, in recent years, Allvac® 718Plus™ alloy (hereafter referred to as 718Plus) [6], Haynes® 282® [7], and AD730 [8] have been introduced which contain more amount of γ′ and can withstand service temperatures above that of IN718.

On the other side, high entropy alloys (HEAs) have spread out an exciting area for designing new alloys with superior properties and new applications [9–12]. Because of the insufficient strength of the single-phase FCC structure of HEAs, some studies were carried out to examine strengthening mechanisms [13]. Precipitation hardening has been widely employed to strengthen several FCC HEAs [14–16]. Zhao et al. [17] indicated that sluggish diffusion in the precipitation-hardened $(NiCoFeCr)_{94}Ti_2Al_4$ HEA, leads to the smaller size of precipitates during aging

✉ Mahmoud Nili-Ahmadabadi
nili@ut.ac.ir

[1] School of Metallurgy and Materials, College of Engineering, University of Tehran, P.O. Box 14395-731, Tehran, Iran

[2] Department of Materials Science and Engineering, POSTECH, Pohang 37673, Republic of Korea

[3] Department of Mechanical Engineering, Ecole de Technologie Superieure (ETS), Montreal, QC H3C 1K3, Canada

and lowers coarsening rate of precipitates at higher temperatures. Recently, some new HEAs containing γ′ phase, as their main strengthening phase, have been introduced as high entropy superalloys (HESAs). Yeh et al. [14] developed a cast HESA ($Ni_{40.7}Al_{7.8}Co_{20.6}Cr_{12.2}Fe_{11.5}Ti_{7.2}$) with nano-sized γ' precipitates with lower density (less than 8 g/cm^3) and lower cost of raw materials than those of conventional Ni-base superalloys. The microstructure of the developed alloy remained stable without any detrimental phases after isothermal aging at 1050 °C for 500 h. Daoud et al. [18] used Thermo-Calc to develop a Ni-rich high-entropy alloy, $Al_8Co_{17}Cr_{17}Cu_8Fe_{17}Ni_{33}$ in which two morphology of γ′ precipitates observed after aging at 700 °C; one with spherical γ′ precipitates less than 20 nm in diameter and the other with elongated morphology less than 350 nm long. With the addition of minor amounts of Ti and Al, He et al. [19] developed a high entropy superalloy with the nominal composition of $(FeCoNiCr)_{94}Ti_2Al_4$ containing nano-sized coherent γ′ precipitates with 645 MPa yield strength and an outstanding 39% elongation. Wang et al. [20] studied a single-phase and aged HEA alloy with the following composition $Al_{0.2}CrFeCoNi_2Cu_{0.2}$ and observed the precipitation of nano-size γ′ precipitates after aging resulted in an increases of 259 and 316 MPa in the yield and ultimate tensile strength, respectively, with a 30.4% elongation. Also, Tsao et al. [21] used Thermo-Calc to design five high entropy superalloys which exhibited stable γ/γ′ microstructures with no Topologically Close-Packed (TCP) phases even after 300 h exposure at 900 °C. They indicated that the higher entropy of the alloy stabilized the microstructure and slowed down or prevented TCP formation.

Superalloys in both cast and wrought conditions, due to a large number of alloying elements in their composition, have higher configurational entropy when compared to other commercial alloys such as steels or titanium alloys [22]. While in the original papers no reference is made to the difference in the configurational entropies of the 718 and 718Plus; calculations reveal that this value is 1.45R (R is the universal gas constant) for 718Plus and 1.29R for IN718. Thereby, the high entropy alloy concept could be used to develop new superalloys with improved microstructural and mechanical properties.

This paper deals with the alloy design scheme and microstructural characterization of a new wrought high entropy superalloy (HES-A1) in the as-cast, homogenized, hot rolled, annealed, and aged conditions following our previous paper, which deals with mechanical properties of this alloy [22]. As the HES-A1 alloy shows promising mechanical properties after aging, this paper mainly focuses on the alloy design and its microstructures in different conditions with aid of optical, scanning and high-resolution transmission electron microscopy and x-ray diffraction.

2 Alloy Design Approach

Because of the widespread use of IN718 superalloy [23–25], its major elements were chosen as a base for designing the new high entropy superalloy. Co was added to enhance the yield strength and the strain hardening capacity [5, 26, 27] while carbon and boron were removed to reduce crack sensitivity [28]. The design objectives for HES-A1 were set to achieve a configurational entropy greater than 1.5R, avoid the formation of δ or γ'' particles and promote that of γ′ instead. Good forming ability, wider hot workability window, and lower or similar density, particularly compared with IN718 alloy, were additional design objectives. On this basis, a list of 20 potential alloys, as reported in "Appendix", using the above-mentioned elements and configurational entropy values of more than 1.5R was prepared and analyzed for phase optimization according to the design objectives.

It is well-known that γ′ strengthened alloys have higher thermal stability than γ″ ones, and γ′ particles in a nickel–iron matrix are usually spherical, and their volume fraction and size are critical in determining their contribution to strengthening [24, 29]. These guidelines were used by Cao et al. [5] and Devaux et al. [27] for developing 718Plus and AD730 alloys, respectively. Both alloys show superior mechanical properties at higher temperatures than IN718 and are characterized by γ′ volume fractions of more than 25% [30, 31]. However, it should be noted that higher γ′ volume fraction deteriorates the hot formability of wrought alloys [32].

To reach a proper volume fraction of γ′ precipitates, the amounts and proportions of Al, Ti, and Nb should be considered as critical parameters. For example, Collier et al. [33] reported that increasing the AI/Ti ratio and/or the AI + Ti content in IN718 alloy improved thermal and mechanical stabilities of the alloy. Chang and Lui [34] found that increasing the Al + Ti content of Waspaloy resulted in increasing yield and tensile strength, and rupture life, at room and high temperature. Cao et al. [6] found that to achieve a predominantly γ′ strengthened alloy, Al + Ti level should be higher than 3 at%. They also found that by increasing the Al/Ti ratio, γ′ would form before γ″, δ, and η, while its precipitation kinetics would be more sluggish. For the development of AD730, Devaux et al. [8] increased the Al/(Ti + Nb) ratio to avoid precipitation of η phase. Figure 1a, b compare Al/Ti and Al/(Ti + Nb) ratio vs. Al + Ti and Ali + Ti + Nb values for some common wrought superalloys. It can be seen that for both plot

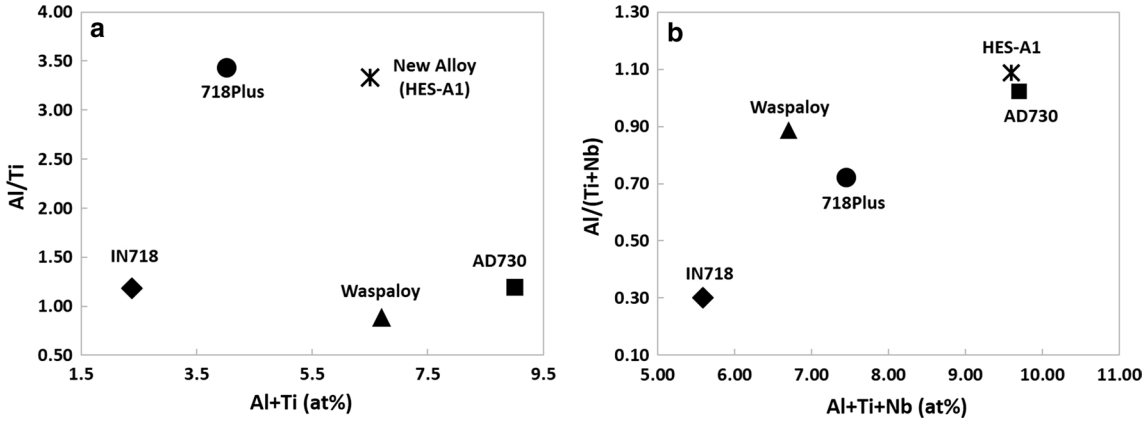

Fig. 1 **a** Al/Ti ratio vs. Al + Ti and **b** Al/(Ti + Nb) ratio versus Al + Ti + Nb for some common wrought superalloys

Table 1 Md values for elements used in this study

Element	Ni	Al	Co	Cr	Fe	Ti	Nb	Mo
Md level, eV	0.717	1.900	0.777	1.142	0.858	2.271	2.117	1.550

improved mechanical properties could be achieved by moving to the right and top of the chart.

The next step in phase formation analysis is related to the presence of TCP phases, which are detrimental to the mechanical properties of superalloys with a high concentration of alloying elements [35–38]. In the present study, the New PhaComp [39] and CALPHAD methods were used to analyze and adjust the proportions of elements with the view to minimize the formation of TCP phases. Specifically, in the New PhaComp method, the average energy levels of d-orbitals (Md) of the transition metals present in the composition of the alloy are important parameters for minimizing the formation of TCP phases. The corresponding Md values for the selected alloying elements entering into the composition of HES-A1 were obtained from Ref. [39] and reported in Table 1.

The Md value of the alloy was then calculated using Eq. 1 [39]:

$$\bar{\mathrm{Md}} = \sum_{i=1}^{n} X_i\left(\mathrm{Md}_i\right), \tag{1}$$

where X_i is the atomic fraction of component i in the alloy and $(Md)_i$ is the Md value of component i.

It can be seen from Table 1 that Ni has the smallest Md value compared with the others. Therefore, as per Eq. (1) substitution of Ni with other elements will increase the Md value of the alloy and increases the propensity for TCP formation. This impact is expected to be higher in the case of high entropy superalloys as the proportion of Ni is lower in comparison with conventional superalloys. On the basis of the above analysis, the Md values for the 20 selected compositions were calculated and found to be in the range of 0.96–1.03. In order to minimize the possible formation of TCP phases, only the alloys with Md values of 0.98 and below were selected for CALPHAD analysis [40].

Hot formability is one of the most important selection factors of wrought superalloys, as the manufacturing process such as forging or rolling requires several steps of hot deformation. However, the hot working window of wrought superalloys is normally between the solvus temperature of δ or γ′ and the solidus of the alloy and often this window is very small. For example, Monajati et al. [41] reported that the hot working window for UDIMET 720 alloy is only 1100 °C to 1150 °C. Such small hot working windows imposes stringent operational limitations that could result in increased quality issues. Therefore, the broadening of the hot working window is a key parameter in the design and selection of a superalloy [37]. While it has commonly been assumed that increasing Al and Ti contents deteriorates the hot formability of superalloys, AD730 alloy with as high as 9 at% Al + Ti content has shown very good formability [27]. It seems that the lower γ′ solvus temperature of AD730 broadened the hot working window and compensated for the higher amount of γ′. Since lower γ′ solvus temperature could cause lower service temperature; therefore, workability and service temperature should be considered together in the analysis [32]. In the present work, using thermodynamic analysis, the proportions of the elements were adjusted for lower γ′ solvus temperature and a higher melting temperature in order to broaden the hot working window of the alloy.

The 20 potential alloys listed in "Appendix" were then classified based on the above-mentioned selection criteria and the new high entropy alloy with a configurational entropy of

Table 2 Chemical composition of the designed high entropy alloy in comparison with IN718, 718Plus, Waspaloy [46] and AD730 [27] (at%)

	Ni	Al	Co	Cr	Fe	Ti	Nb	Mo	W	C	P	B	Zr	Md	ΔS/R
New Alloy	46.4	5.0	5.0	21.2	15.0	1.5	3.1	2.8	–	–	–	–	–	0.98	1.51
IN718	53.57	0.97	–	20.23	18.73	1.21	3.38	1.76	–	0.12	0.01	0.02	–	0.92	1.29
718Plus	51.07	3.12	8.88	20.12	10.41	0.85	3.41	1.70	0.32	0.10	0.01	0.02	–	0.94	1.45
Waspaloy	56.95	2.74	12.79	21.23	–	3.57	–	2.52	–	0.17	0.01	0.03	–	0.93	1.15
AD730	57.90	4.79	8.28	17.33	4.11	4.08	0.68	1.86	0.84	0.07	–	0.05	0.02	0.94	1.37

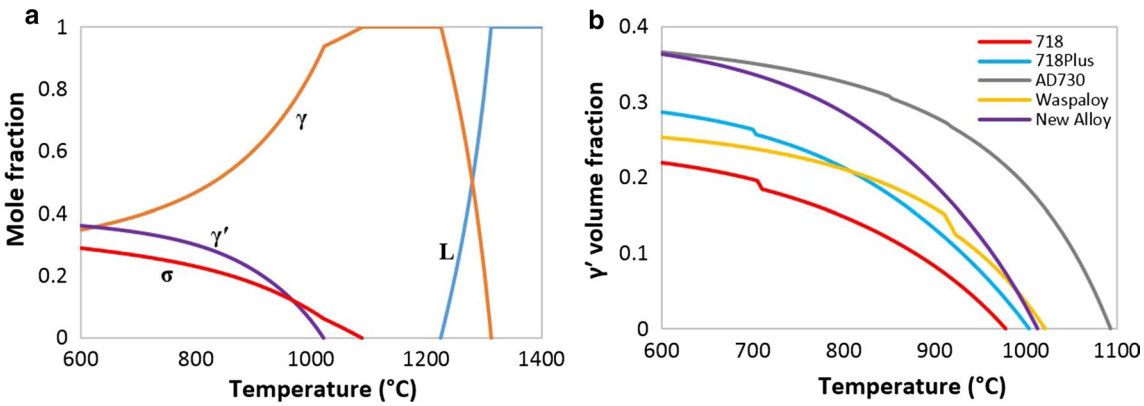

Fig. 2 **a** Calculated phase fraction plot for HES-A1 and **b** the maximum amount of γ′ phase and solvus temperature in most popular wrought superalloys calculated by Thermo-Calc software

Table 3 Density of most popular wrought superalloys

Alloy	IN718 [48]	718Plus [49]	Waspaloy [50]	AD730 [51]	HES-A1
Density (kg/m3)	8.22	8.25	8.20	8.20	8.05
Δρ (%) (compared with IN718)	0.00	+0.36	−0.24	−0.24	−2.07

1.54R and the chemical composition presented in Table 2 was selected. In the same table, the chemical composition, Md, and ΔS/R values of IN718, 718Plus, Waspaloy and AD730 are also presented for comparing purposes. As shown in Fig. 1, in the newly designed alloy, the amount of Al + Ti is near that of Waspaloy but its Al/Ti ratio is significantly higher. Compared to 718Plus, HES-A1 has the same Al/Ti ratio but contains nearly 2.5 at% more Al + Ti. It should be noted that the calculated Md value of HES-A1 is slightly higher than those of the other alloys. The calculated phase diagram reported in Fig. 2a, predicts a primarily γ/γ′ structure, with the formation of the σ phase at 1090 °C and at lower temperatures. The formation of σ phase has been predicted by the Thermo-Calc software for superalloys such as 718 [42] and 718Plus [43], however, because of the very sluggish precipitation of the σ-phase, it could not be observed in the microstructure until after long time exposure at high temperatures [44]. Also, as reported by Choi et al. [45] while the formation of the sigma phase had been predicted by the thermodynamic software, its presence was not detected in the microstructures of cast or heat treated of some high entropy alloys.

Figure 2b shows the calculated solvus temperature and the maximum amount of γ′ in the four reference superalloys, selected in this study. It can be seen that HES-A1 has similar γ′ volume fraction to AD730 but significantly higher than Waspaloy, IN718, and 718Plus; suggesting better mechanical properties compared to the last three alloys. On the other hand, its γ′ solvus temperature of 1010 °C is closer to those of 718Plus (1004 °C) and Waspaloy (1013 °C) and lower than that of AD730 (1090 °C) indicating a broader workability window than AD730. The γ′ solvus temperatures of a superalloy depends on its chemical composition and could be estimated using thermodynamic software or linear regression analysis of experimental data for a series of nickel-based superalloys provide in [47].

Another important consideration in the design of the proposed alloy was to achieve a lower density alloy than the main commercial alloys. In this study, the increased Al and

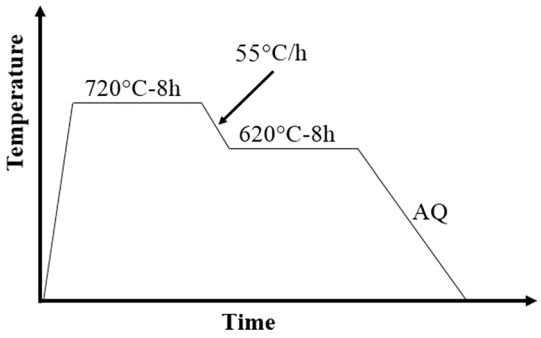

Fig. 3 Double-aging cycle for HES-A1 similar to standard aging of IN718

Ti contents and reduced Ni and elimination of W from the composition of the alloy resulted in a lower density compared to the main commercial wrought superalloys, as indicated in Table 3.

3 Experimental

The alloy was produced by double vacuum melting (vacuum induction melting and arc melting, VIM/VAR) which ensures excellent micro-cleanliness and tight compositional control. After characterization of the as-cast condition, ingots were homogenized at 1145 °C for 24 h in order to dissolve the Laves phase. The homogenized ingots with an initial thickness of 26 mm were successfully hot rolled at 1015 °C using a speed of 3 rpm to a final thickness of 16 mm. For the first pass, the ingot was hot rolled with 20% reduction in thickness and for the subsequent six passes; about 15% reduction in thickness was applied, per pass. A reheating period of 5 min was considered between the subsequent passes. After hot rolling, the ingot was annealed at 1145 °C for 1 h. Double-aging, which is commonly used in superalloys with the thermal cycle shown in Fig. 3 was applied to the annealed samples. X-ray diffraction (XRD) patterns were obtained using Cu Kα radiation and a scan step size of 0.02°. Room-temperature density was determined with a device using the Archimedes method.

The specimens were mechanically polished by SiC papers of 400, 600, 800, and 1200 grits, followed by diamond suspensions of 3 and 1 µm. The polished surfaces were etched with an etchant composed of 5 ml of lactic acid, 3 ml of nitric acid, and 0.2 ml of HF to reveal microstructure in the optical and scanning electron microscopes. The microstructure of hot rolled and annealed samples were characterized using a field emission scanning electron microscope (FE-SEM, Quanta 3D FEG, FEI) equipped with an EDAX.

To prepare specimens for transmission electron microscope (TEM), after an initial thinning of the specimens by SiC papers up to 100 µm, 3 mm diameter discs were punched out from the 100 µm foil using a Gatan punch and were electro-polished using a Struers TenuPol-5 in an electrolyte of 10% Perchloric acid and 90% Acetic acid. A voltage of 27 V and a current of 31 mA were used. A JEOL JEM 2100F equipment operating at an acceleration voltage of 200 kV was used for TEM imaging, acquiring SAED patterns, and HR-TEM analysis.

4 Results and Discussion

The as-cast material with dimensions of 140 mm × 25 mm × 12 mm had a dendritic structure with an average secondary dendrite arm spacing of about

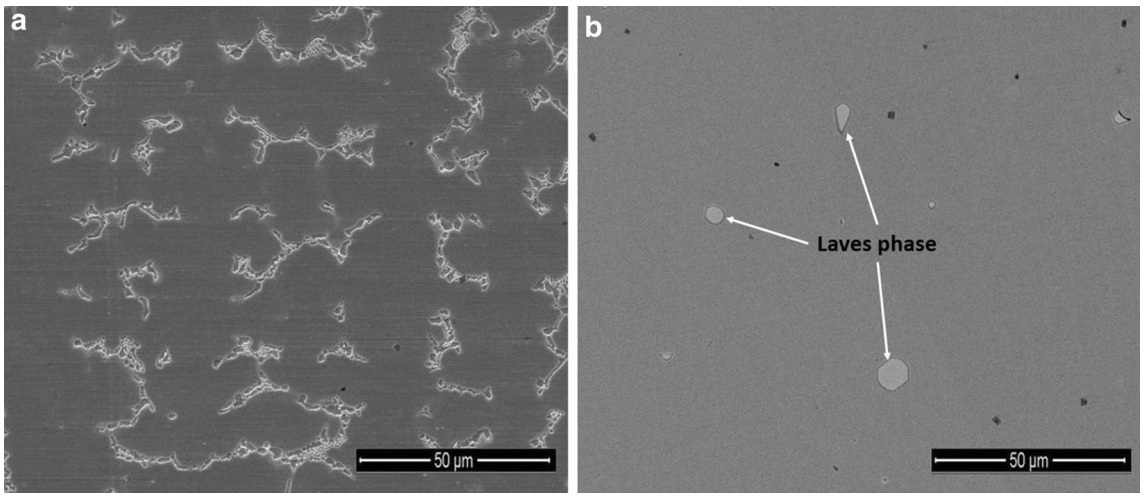

Fig. 4 SE-SEM image of the **a** as-cast sample and **b** homogenized sample with small Laves precipitates

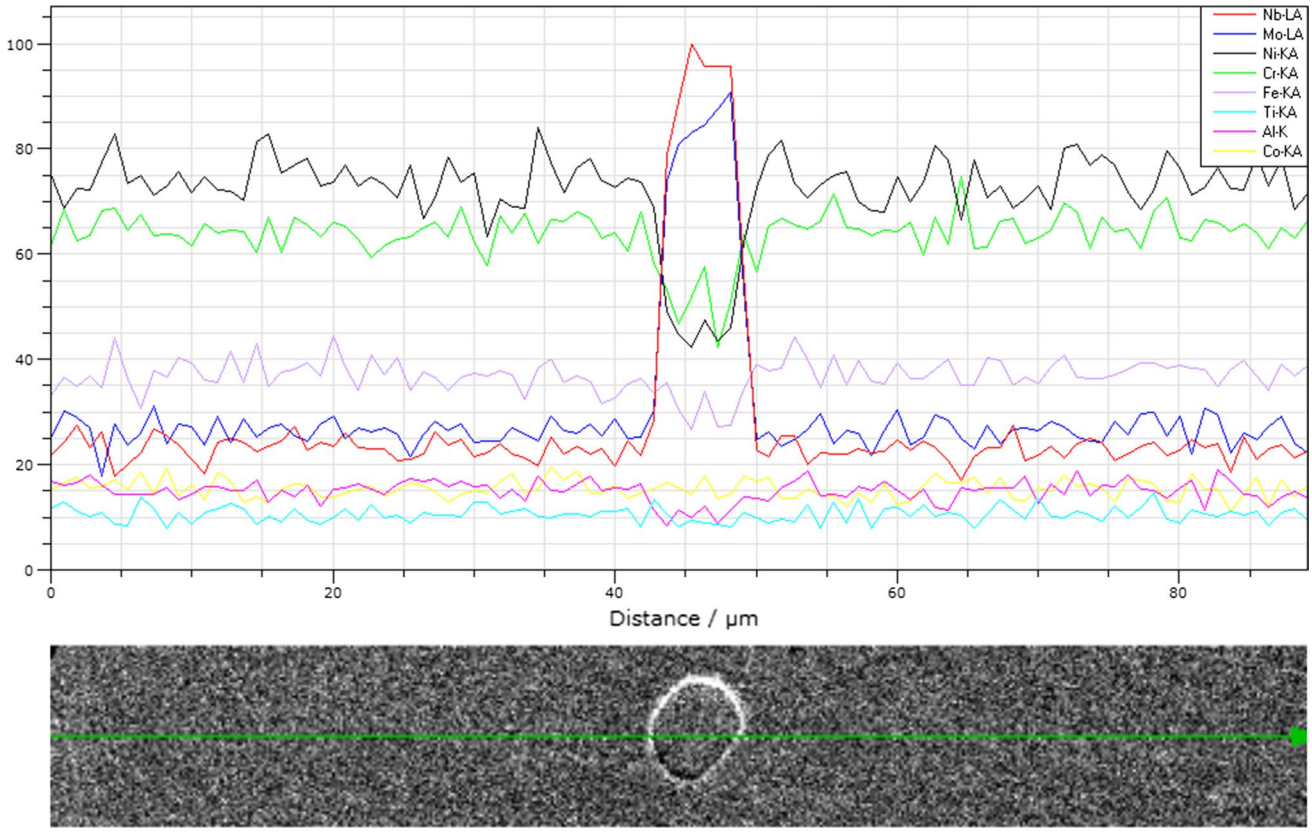

Fig. 5 Distribution of the elements around the Laves particle after homogenization treatment

Table 4 Chemical composition of Laves particle after homogenization treatment (at%)

	Ni	Al	Co	Cr	Fe	Ti	Nb	Mo
Laves particle	33.68	4.72	5.12	17.80	14.88	1.43	14.51	7.86

20 µm. White discontinuous networks of intermetallic Laves phases were observed in the center of the inter-dendritic region as shown in Fig. 4a. The presence of Laves phases is common in Nb-bearing alloying such as 718, 625, and 909 alloys [52]. Image analysis of SEM images indicates that the Laves phase volume fraction in the as-cast microstructure was 5.5%. Comparing to IN718, the volume fraction of Laves phase changed related to the cooling rate [53], but similar networks of intermetallic Laves phases has been observed and its volume fraction varies from 3.2 [54] to 5.4% [55] for the as-cast condition in different works. In 718Plus the volume fraction of the Laves phase in thin and thick sections has been reported to be 1.6%–4.5%, respectively [56]. After homogenization heat treatment at 1145 °C for 24 h, the microstructural analysis indicated that the volume fraction of Laves phases reached below 0.3 vol% in the form of very small and dispersed precipitates (Fig. 4b). The black spots in Fig. 4b, which are less than one micron in size, demonstrate the shrinkage porosity. The volume fraction of porosity is less than 0.1% after homogenization treatments. Some pores are from casting and some from homogenization treatment. As reported earlier in [57] when the Laves phase goes into solution, some porosity may result that are not interconnected and are quickly healed during hot working.

Using the EDAX analysis, elemental distribution around one of the small precipitates after homogenization treatment is shown in Fig. 5 and the average chemical composition of these particles is shown in Table 4. The EDAX analysis shows that Laves precipitates that remain after homogenization are rich in Nb and Mo. These observations are in agreement with those reported by several authors on various types of superalloys [58–61]. It should be noted that no

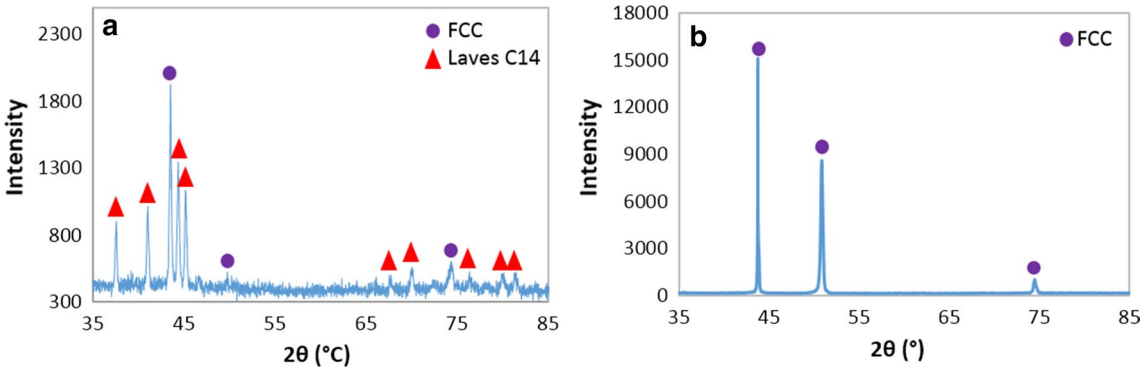

Fig. 6 XRD patterns of the **a** as-cast sample and **b** homogenized sample

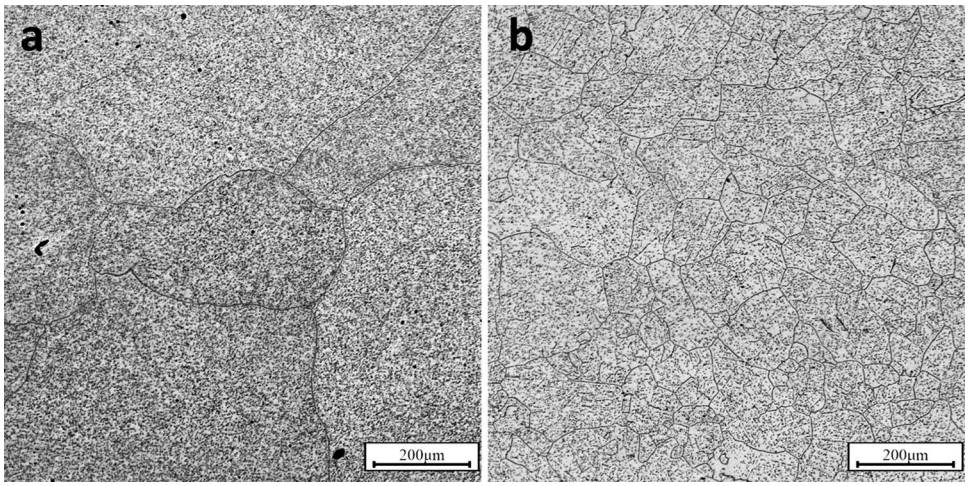

Fig. 7 **a** Optical image of the sample before hot rolling and after hot rolling at 1015 °C and annealing at 1145 °C for 1 h

Sigma phase was detected after casting or homogenization of HES-A1.

Figures 6a, b show the XRD patterns of the as-cast and homogenized samples, which confirm the presence of Laves phases in the as-cast sample and single FCC phase in the homogenized one. Since the volume fraction of Laves phases reached below 0.3 vol% after homogenization, such a low content of Laves phase cannot be detected by XRD [62].

A lattice parameter of 0.3576 nm was measured for solid solution gamma phase that, as expected, is larger than the lattice parameter of pure Ni, which is 0.3517 nm [63].

Figure 7 shows optical microscopy images of the ingot before and after hot rolling at 1015 °C and annealing at 1145 °C for 1 h. After homogenization, the grain size of the ingot was in the range of 200 μm to 2 mm while the most grains were larger than 1 mm. Some abnormality in grain size was observed which has been reported earlier for IN718 during forging [64, 65]. One of the small grains could be seen in the center of Fig. 7a. The results clearly indicate that hot rolling resulted in a significant grain refinement of the large homogenized grains into smaller ones with an average grain size of about 69 μm. Most of the grains were more than 1 mm in diameter before rolling, while the grain size was within the 30 to 100 μm interval after hot rolling. It is well known that Ni-based superalloys have low or medium

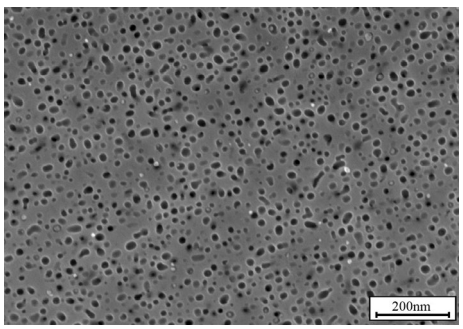

Fig. 8 FE-SEM image of HES-A1 after double aging

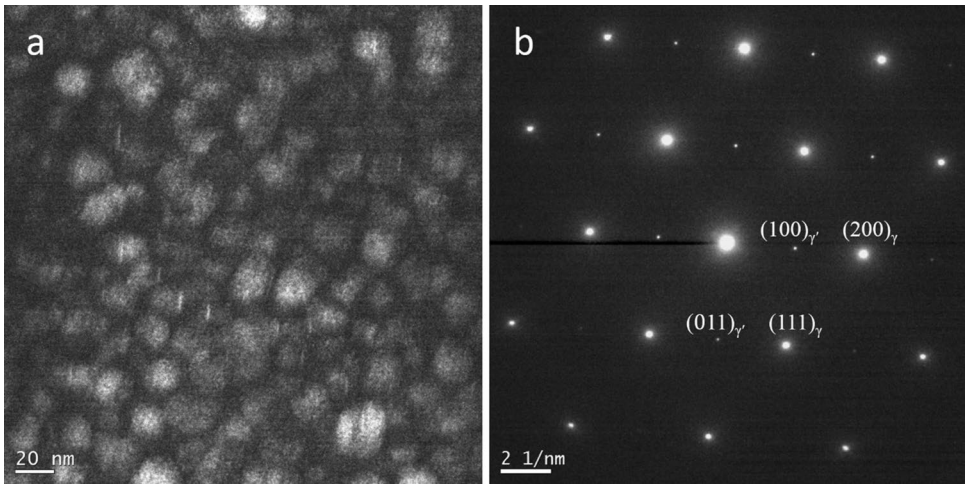

Fig. 9 **a** Bright field TEM of HES-A1 after aging, **b** SAD pattern of γ/γ′ along < 011 > FCC zone axes of the aged microstructure

stacking fault energy and as a result, dynamic recrystallization occurs very rapidly during hot deformation bringing grain refinement in the microstructure [66]. As shown in Fig. 7b, the significant grain refinement of HES-A1 after hot rolling could indicate that HES-A1 has low to medium stacking fault energy.

The morphology and distribution of γ′ precipitates were examined using FE-SEM and TEM. To this end, similar to the standard aging cycle of IN718 alloy, the hot rolled sample was held for 8 h at 720 °C, followed by cooling at a rate of 55 °C/h, and then was held for 8 h at 620 °C before being air cooled to room temperature. Figures 8 shows FE-SEM image of the double-aged sample in secondary electron imaging mode (SE), where a uniform distribution of nano-size γ′ precipitates throughout the γ matrix can be observed. Using ImageJ software and FE-SEM images in SE mode, the volume fraction of γ′ in HES-A1 was determined to be around 31%, which is slightly lower than the predicted value by the Thermo-Calc software (Fig. 2a). The very small size of γ′ precipitates in Fig. 8 clearly shows that TEM observation is the most appropriate technique for their characterization.

Figure 9a shows the bright field TEM image of the double-aged sample with electron diffraction pattern along <011> FCC zone axis. Spherical shape γ′ precipitates with uniform distribution and the average size of 18.20 ± 3.09 nm after about 18 h of aging could be seen in these images. Selected area electron diffraction (SAED) was conducted in order to identify crystallographic structures of matrix and precipitates and the results are presented in Fig. 9b. The bright spots in the SAED image correspond to the γ and γ′ phase with superlattice spots from the γ′ phase (because of the ordering within the γ′ precipitates). The absence of any additional spot in the diffraction pattern indicates the absence of any incoherent precipitation. Based on the microstructural characterizations of HES-A1, it could be concluded that similar to the other Nb-bearing superalloys, such as IN718, and 718Plus, the as-cast microstructures of HES-A1 has the same level of the Laves phase. However, because of the absence of δ phase at the grain boundaries and the absence of γ″ as a strengthening phase (in the case of IN718) [43], their aged microstructures are different. Moreover, HES-A1 has been designed deliberately so that, with a higher Al/(Ti + Nb) ratio and higher proportion of Al + Ti + Nb it could be fully strengthened by γ′ precipitation, similar to the aged conditions of the AD730 and Waspaloy. Nevertheless, it should be emphasized that because of the Nb content of HES-A1, its as-cast microstructure is different from that of the AD730 and Waspaloy. On the other hand, γ′ precipitates in HES-A1 are monomodal and have relatively smaller size when compared to other wrought superalloys such as AD730 or Waspaloy [67, 68].

Figure 10a shows a high-resolution TEM image of the interface between the γ′ precipitate and γ matrix. It could be seen that the γ′ precipitates are not completely spherical at higher magnifications and facets surround some of these precipitates. The corresponding fast Fourier transform (FFT) patterns of γ′ and the γ matrix are presented in Figs. 10b, c, respectively, which are accurately consistent with the results of the diffraction pattern. The FFT patterns confirm the existence of γ′ precipitates and γ matrix in the left and right side of the Fig. 10a, respectively. Considering the FFT patterns of the γ and γ′ phases, {100} and {111} facets could be observed from A to B and from B to C in Fig. 10a, respectively. Faceted γ′, at such small sizes, have been reported by Whitmore et al. [69] for the first time after double aging of the 718Plus alloy. The results obtained in the present work, with the

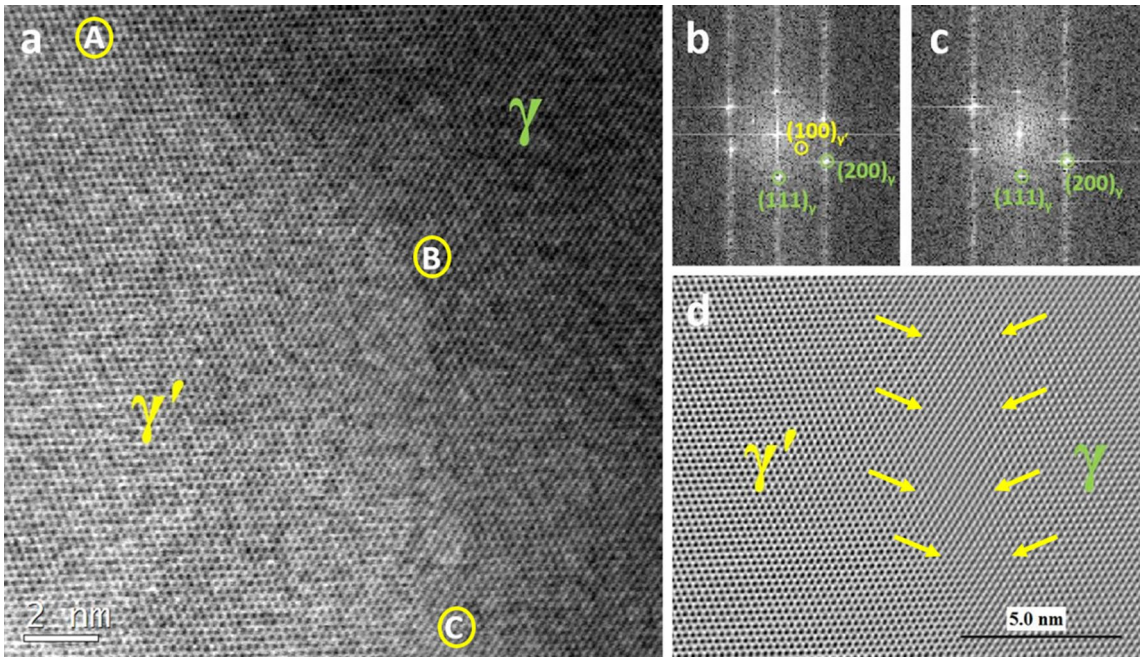

Fig. 10 **a** High-resolution TEM image showing the γ/γ′ interface, corresponding fast Fourier transform (FFT) patterns of **b** γ′ precipitate and **c** γ matrix and **d** inverse transform of the masked {111} facet of the interface

clear distinction of the interface, further confirm their formation.

To further analyze the coherency level of the γ/γ′ interface, the GATAN digital micrograph software was used along the {111} facet of the interface in Fig. 10a. To this end, a mask was applied in DigitalMicrograph after Fourier transform of the high-resolution images and then, an inverse transform of the masked regions was used. Figure 10d shows an illustrative example of a region of about 2 nm of the γ/γ′ interface where a very high coherency can be observed. As reported by Donachie in precipitate strengthened alloys where deformation is impeded by the precipitates, the optimal condition is for matrix and precipitate to have almost same size crystal lattices [1]. In fact, a lower misfit produces minimum elastic strain energy and as a result, the rate of precipitate coarsening at elevated temperatures will be reduced [70].

5 Conclusions

In this work, a new wrought high entropy superalloy (designated as HES-A1) was developed using high entropy alloy concept, CALPHAD, and Phacomp methods. The alloy is characterized with monomodal nano-size γ′ precipitates, with a high degree of γ/γ′ interface coherency. The absence of γ″ in the microstructure is indicative of its higher thermal stability when compared to IN718 alloy. A homogenization heat treatment process was developed that allowed reducing the Laves phase content to very low levels. The density, hot workability window, and γ′ solvus temperature of HES-A1 are similar or better than common wrought superalloys such as IN718, 718Plus, Waspaloy, and AD730. The successful hot rolling, with significant grain refinement, of the developed alloy, confirm its potential for application where rolled or forged products are needed.

Acknowledgements This project was defined in the framework of the collaboration program between University of Tehran, ETS, and POSTECH. A. Shafiee and M. Nili-Ahmadabadi would like to express their appreciations to Iran National Science Foundation. In addition, A. Shafiee would like to acknowledge ETS-CM2P for financial support, POSTECH for access to characterization equipment and Jongun Moon for helping with TEM samples preparation and operating XRD machine.

Table 5 List of the 20 potential alloys compositions used in the preliminary analysis

	Ni	Al	Co	Cr	Fe	Ti	Nb	Mo	ΔS/R	Md
A1	47.7	4.0	5.0	21.2	15.0	1.2	3.1	2.8	− 1.51	0.96
A2	46.7	5.0	5.0	21.2	15.0	1.2	3.1	2.8	− 1.53	0.98
A3	47.7	5.0	5.0	21.2	14.0	1.2	3.1	2.8	− 1.52	0.97
A4	46.7	5.0	5.0	21.2	15.0	1.2	3.1	2.8	− 1.53	0.98
A5	45.7	5.0	5.0	21.2	16.0	1.2	3.1	2.8	− 1.54	0.98
A6	44.7	5.0	5.0	21.2	17.0	1.2	3.1	2.8	− 1.55	0.98
A7	43.7	5.0	5.0	21.2	18.0	1.2	3.1	2.8	− 1.56	0.98
A8	42.7	5.0	5.0	21.2	19.0	1.2	3.1	2.8	− 1.57	0.98
A9	46.7	5.0	5.0	21.2	15.0	1.2	3.1	2.8	− 1.53	0.98
A10	47.7	5.0	5.0	21.2	15.0	1.2	3.1	1.8	− 1.50	0.97
A11	45.7	5.0	5.0	21.2	15.0	1.2	3.1	3.8	− 1.56	0.98
A12	45.7	5.0	5.0	21.2	15.0	1.2	3.1	4.8	− 1.58	1.00
A13	49.9	5.0	5.0	17.0	16.0	1.2	3.1	2.8	− 1.50	0.96
A14	49.9	5.0	5.0	18.0	15.0	1.2	3.1	2.8	− 1.50	0.96
A15	48.9	5.0	5.0	19.0	15.0	1.2	3.1	2.8	− 1.51	0.97
A16	47.9	5.0	5.0	20.0	15.0	1.2	3.1	2.8	− 1.52	0.97
A17	46.9	5.0	5.0	20.0	15.0	2.2	3.1	2.8	− 1.55	0.99
A18	46.9	5.0	5.0	20.0	15.0	2.2	3.1	2.8	− 1.55	0.99
A19	46.4	5.0	5.0	21.2	15.0	1.5	3.1	2.8	− 1.54	0.98
A20	45.4	5.0	5.0	21.2	15.0	2.5	3.1	2.8	− 1.57	1.00

Appendix

See Table 5.

References

1. M.J. Donachie, S.J. Donachie, *Superalloys—A Technical Guide* (ASM International, Russel Township, 2002)
2. E.A. Loria, The status and prospects of alloy 718. JOM J. Miner. Met. Mater. Soc. **40**, 36–41 (1988)
3. L. Geng, Y.-S. Na, N.-K. Park, Precipitation behavior of hot-extruded alloy 718 during isothermal treatment. Met. Mater. **5**, 389–393 (1999). https://doi.org/10.1007/bf03187763
4. Y.-S. Na, J.-T. Yeom, N.-K. Park, J.-Y. Lee, Prediction of microstructure evolution during high temperature blade forging of a Ni–Fe based superalloy, Alloy 718. Met. Mater. Int. **9**, 15–19 (2003). https://doi.org/10.1007/BF03027224
5. R.L. Kennedy, ALLVAC 718PLUS, superalloy for the next forty years. Superalloys **718**(706), 1–14 (2005). https://doi.org/10.7449/2005/superalloys_2005_1_14
6. W.D. Cao, R.L. Kennedy, New developments in wrought 718-type superalloys. Acta Metall. Sin. **18**, 39–46 (2005)
7. H. Matysiak, M. Zagorska, J. Andersson, A. Balkowiec, R. Cygan, M. Rasinski, M. Pisarek, M. Andrzejczuk, K. Kubiak, K.J. Kurzydlowski, Microstructure of Haynes® 282® superalloy after vacuum induction melting and investment casting of thin-walled components. Materials **6**(2013), 5016–5037 (2013). https://doi.org/10.3390/ma6115016
8. A. Devaux, B. Picqué, M.F. Gervais, E. Georges, T. Poulain, P. Héritier, AD730™-a new nickel-based superalloy for high temperature engine rotative parts, *Superalloys* (Wiley, Hoboken, 2012), pp. 911–919. https://doi.org/10.1002/9781118516430.ch100
9. M.J. Jang, S.-H.H. Joo, C.-W.W. Tsai, J.-W.W. Yeh, H.S. Kim, Compressive deformation behavior of CrMnFeCoNi high-entropy alloy. Met. Mater. Int. **22**, 982–986 (2016). https://doi.org/10.1007/s12540-016-6304-2
10. D.B. Miracle, O.N. Senkov, A critical review of high entropy alloys and related concepts. Acta Mater. **122**, 448–511 (2017). https://doi.org/10.1016/j.actamat.2016.08.081
11. M. Li, J. Gazquez, A. Borisevich, R. Mishra, K.M. Flores, Evaluation of microstructure and mechanical property variations in AlxCoCrFeNi high entropy alloys produced by a high-throughput laser deposition method. Intermetallics **95**, 110–118 (2018). https://doi.org/10.1016/J.INTERMET.2018.01.021
12. Y. Zhang, *High-Entropy materials- A Brief Introduction* (Springer, Singapore, 2019)
13. Z.P.P. Lu, H. Wang, M.W.W. Chen, I. Baker, J.W.W. Yeh, C.T.T. Liu, T.G.G. Nieh, An assessment on the future development of high-entropy alloys: summary from a recent workshop. Intermetallics **66**, 67–76 (2015). https://doi.org/10.1016/j.intermet.2015.06.021
14. T. Tsao, Y. Chang, K. Chang, J. Yeh, M. Chiou, S. Jian, C. Kuo, W. Wang, H. Murakami, H. Murakami, Developing new type of

high temperature alloys-high entropy superalloys. Int. J. Metall. Mater. Eng. (2015). https://doi.org/10.15344/2455-2372/2015/107
15. J.Y. He, H. Wang, Y. Wu, X.J. Liu, H.H. Mao, T.G. Nieh, Z.P. Lu, Precipitation behavior and its effects on tensile properties of FeCoNiCr high-entropy alloys. Intermetallics **79**, 41–52 (2016). https://doi.org/10.1016/j.intermet.2016.09.005
16. T. Bhattacharjee, I.S. Wani, S. Sheikh, I.T. Clark, T. Okawa, S. Guo, P.P. Bhattacharjee, N. Tsuji, Simultaneous strength-ductility enhancement of a nano-lamellar AlCoCrFeNi2.1 eutectic high entropy alloy by cryo-rolling and annealing. Sci. Rep. **8**, 1–8 (2018). https://doi.org/10.1038/s41598-018-21385-y
17. Y.Y. Zhao, H.W. Chen, Z.P. Lu, T.G. Nieh, Thermal stability and coarsening of coherent particles in a precipitation-hardened (NiCoFeCr)94Ti2Al4high-entropy alloy. Acta Mater. **147**, 184–194 (2018). https://doi.org/10.1016/j.actamat.2018.01.049
18. H.M. Daoud, A. Manzoni, R. Völkl, N. Wanderka, U. Glatzel, Microstructure and tensile behavior of Al8Co17Cr17Cu8Fe17Ni33 (at.%) high-entropy alloy. JOM **65**, 1805–1814 (2013). https://doi.org/10.1007/s11837-013-0756-3
19. J.Y. He, H. Wang, H.L. Huang, X.D. Xu, M.W. Chen, Y. Wu, X.J. Liu, T.G. Nieh, K. An, Z.P. Lu, A precipitation-hardened high-entropy alloy with outstanding tensile properties. Acta Mater. **102**, 187–196 (2016). https://doi.org/10.1016/j.actamat.2015.08.076
20. Z.G. Wang, W. Zhou, L.M. Fu, J.F. Wang, R.C. Luo, X.C. Han, B. Chen, X.D. Wang, Effect of coherent L12nanoprecipitates on the tensile behavior of a fcc-based high-entropy alloy. Mater. Sci. Eng., A **696**, 503–510 (2017). https://doi.org/10.1016/j.msea.2017.04.111
21. T.K. Tsao, A.C. Yeh, H. Murakami, The microstructure stability of precipitation strengthened medium to high entropy superalloys. Metall. Mater. Trans. A Phys. Metall. Mater. Sci. **48**, 2435–2442 (2017). https://doi.org/10.1007/s11661-017-4037-6
22. M.C. Gao, J.W. Yeh, P.K. Liaw, Y. Zhang, *High-Entropy Alloys: Fundamentals and Applications*, 1st edn. (Springer, Berlin, 2016). https://doi.org/10.1007/978-3-319-27013-5
23. M. Azarbarmas, M. Aghaie-Khafri, J.M. Cabrera, J. Calvo, Microstructural evolution and constitutive equations of Inconel 718 alloy under quasi-static and quasi-dynamic conditions. Mater. Des. **94**, 28–38 (2016). https://doi.org/10.1016/j.matdes.2015.12.157
24. G.D. Smith, S.J. Patel, The role of niobium in wrought precipitation-hardened nickel-base alloys. Superalloys **718**, 625–706 (2005). https://doi.org/10.7449/2005/superalloys_2005_135_154
25. P.E.G. Wagenhuber, V.B. Trindade, U. Krupp, The role of oxygen-grain-boundary diffusion during intercrystalline oxidation and intergranular fatigue crack propagation in alloy 718. Superalloys **718**, 625–706 (2005). https://doi.org/10.7449/2005/superalloys_2005_591_600
26. C. Tian, G. Han, C. Cui, X. Sun, Effects of Co content on tensile properties and deformation behaviors of Ni-based disk superalloys at different temperatures. Mater. Des. **88**, 123–131 (2015). https://doi.org/10.1016/j.matdes.2015.08.114
27. A. Devaux, B. Picque, M.F. Gervais, E. Georges, T. Poulain, P. Heritier, AD730TM—A new Nickel-Based Superalloy for High Temperature Engine Rotative Parts, in *Superalloys 2012 12th Int. Symp. Superalloys* (2012) pp. 911–919
28. M. Sundararaman, P. Mukhopadhyay, S. Banerjee, Carbide precipitation in nickel base superalloys 718 and 625 and their effect on mechanical properties. Superalloys **718**, 625–706 (1997). https://doi.org/10.7449/1997/superalloys_1997_367_378
29. E.H. Van der Molen, J.M. Oblak, O.H. Kriege, Control of γ′ particle size and volume fraction in the high temperature superalloy Udimet 700. Metall. Trans. **2**, 1627–1633 (1971). https://doi.org/10.1007/bf02913886
30. K. Löhnert, F. Pyczak, Microstructure evolution in the nickel base superalloy Allvac®718PlusTM, in *7th Int. Symp. Superalloy 718 Deriv.* (2010) pp. 877–891
31. L. Thébaud, P. Villechaise, J. Cormier, C. Crozet, A. Devaux, D. Béchet, J.-M. Franchet, A. Organista, F. Hamon, Relationships between microstructural parameters and time-dependent mechanical properties of a new nickel-based superalloy AD730™. Metals (Basel) **5**, 2236–2251 (2015). https://doi.org/10.3390/met5042236
32. Z. Bi, X. Lv, J. Zhang, Solutions for the "difficult-to-deform" wrought superalloys. MATEC Web Conf. **14**, 07002 (2014). https://doi.org/10.1051/matecconf/20141407002
33. J.P. Collier, S.H. Wong, J.K. Tien, J.C. Phillips, The effect of varying AI, Ti, and Nb content on the phase stability of INCONEL 718. Metall. Trans. A **19**, 1657–1666 (1988). https://doi.org/10.1007/BF02645133
34. K.M. Chang, X. Liu, Effect of γ′ content on the mechanincal behavior of the WASPALOY alloy system. Mater. Sci. Eng. A **308**, 1–8 (2001). https://doi.org/10.1016/S0921-5093(00)02042-6
35. F. Sun, J.X. Zhang, Topologically close-packed phase precipitation in Ni-based superalloys. Adv. Mater. Res. **320**, 26–32 (2011). https://doi.org/10.4028/www.scientific.net/AMR.320.26
36. A.S. Wilson, Formation and effect of topologically close-packed phases in nickel-base superalloys. Mater. Sci. Technol. (United Kingdom) **33**, 1108–1118 (2017). https://doi.org/10.1080/02670836.2016.1187335
37. M.J. Donachie, S.J. Donachie, *Superalloys*, 2nd edn. (ASM International, Materials Park, OH, 2002)
38. J. Belan, GCP and TCP Phases Presented in Nickel-base Superalloys. Mater. Today Proc. **3**, 936–941 (2016). https://doi.org/10.1016/j.matpr.2016.03.024
39. M. Morinaga, N. Yukawa, H. Adachi, H. Ezaki, New phacomp and its applications to alloy design, superalloys 1984 (Fifth Int. Symp. (1984) pp. 523–532. https://doi.org/10.7449/1984/superalloys_1984_523_532
40. B.D. Conduit, N.G. Jones, H.J. Stone, G.J. Conduit, Design of a nickel-base superalloy using a neural network. Mater. Des. **131**, 358–365 (2017). https://doi.org/10.1016/j.matdes.2017.06.007
41. H. Monajati, A.K. Taheri, M. Jahazi, S. Yue, Deformation characteristics of isothermally forged UDIMET 720 nickel-base superalloy. Metall. Mater. Trans. A **36**, 895–905 (2005). https://doi.org/10.1007/s11661-005-0284-z
42. F.R. Caliari, N.M. Guimarães, D.A.P. Reis, A.A. Couto, C. de Moura Neto, K.C.G. Candioto, Study of the secondary phases in inconel 718 aged superalloy using thermodynamics modeling. Key Eng. Mater. **553**, 23–28 (2013). https://doi.org/10.4028/www.scientific.net/KEM.553.23
43. X. Xie, G. Wang, J. Dong, C. Xu, W.-D. Cao, R. Kennedy, Structure stability study on a newly developed nickel-base superalloy—Allvac 718Plus. Superalloys **718**, 625–706 (2005). https://doi.org/10.7449/2005/superalloys_2005_179_191
44. S. Zhao, X. Xie, G.D. Smith, S.J. Patel, Microstructural stability and mechanical properties of a new nickel-based superalloy. Mater. Sci. Eng. A **355**, 96–105 (2003). https://doi.org/10.1016/S0921-5093(03)00051-0
45. W.-M. Choi, S. Jung, Y.H. Jo, S. Lee, B.-J. Lee, Design of new face-centered cubic high entropy alloys by thermodynamic calculation. Met. Mater. Int. **23**, 839–847 (2017). https://doi.org/10.1007/s12540-017-6701-1
46. W. Di Cao, R. Kennedy, Role of Chemistry in 718-Type Alloys-Allvac 718Plus Alloy Development, in *Superalloys 2004* (2004) pp. 91–99
47. P. Caron, High γ′ solvus new generation nickel-based superalloys for single crystal turbine blade applications. Superalloys **2000**, 737–746 (2000). https://doi.org/10.7449/2000/superalloys_2000_737_746

48. INCONEL® Alloy 718 Data Sheet- Special Metals Company (2007). http://www.specialmetals.com/tech-center/alloys.html
49. Technical Data Sheet- 718Plus ®, ATI Properties, Inc. (2013). https://www.atimetals.com/Products/Documents/datasheets/nickel-cobalt/nickel-based/ati_718plus_tds_en_v3.pdf
50. P. Features, N. Composition, HAYNES ® Waspaloy alloy, Haynes International (2017). http://www.haynesintl.com/alloys/alloy-portfolio_/High-temperature-Alloys/haynes-waspaloy-alloy/physical-properties
51. AD730®- New Ni-based Superalloy for High Temperature Applications (2017). https://www.aubertduval.com/wp-media/uploads/sites/2/2017/07/2017_Brochure_AD730.pdf. Accessed May 4 2018
52. C.H. Radhakrishna, K. Prasad Rao, The formation and control of Laves phase in superalloy 718 welds. J. Mater. Sci. **32**, 1977–1984 (1997). https://doi.org/10.1023/a:1018541915113
53. S.G.K. Manikandan, D. Sivakumar, K.P. Rao, M. Kamaraj, Effect of weld cooling rate on Laves phase formation in Inconel 718 fusion zone. J. Mater. Process. Technol. **214**, 358–364 (2014). https://doi.org/10.1016/j.jmatprotec.2013.09.006
54. Z. Miao, A. Shan, W. Wang, J. Lu, W. Xu, H. Song, Quantitative characterization of two-stage homogenization treatment of alloy 718, in *7th Int. Symp. Superalloy 718 Deriv.* (2010), pp. 107–115. https://doi.org/10.1002/9781118495223.ch7
55. M.J. Cieslak, G.A. Knorovsky, T.J. Headley, A.D. Romig Jr, The solidification metallurgy of alloy 718 and other Nb-containing superalloys. Superalloys **718**, 59–68 (1989). https://doi.org/10.7449/1989/superalloys_1989_59_68
56. T. Howson, J. Andersson, *Homogenization of Precipitation Hardening Nickel Based Superalloys*, (2012) pp. 4–6
57. R.M. Forbes Jones, L.A. Jackman, The structural evolution of superalloy ingots during hot working. JOM **51**, 27–31 (1999). https://doi.org/10.1007/s11837-999-0007-9
58. Z.J. Miao, A.D. Shan, Y.B. Wu, J. Lu, Y. Hu, J.L. Liu, H.W. Song, Effects of P and B addition on as-cast microstructure and homogenization parameter of Inconel 718 alloy. Trans. Nonferrous Met. Soc. China **22**, 318–323 (2012). https://doi.org/10.1016/s1003-6326(11)61177-1. **(English Ed.)**
59. M.G. Burke, M.K. Miller, Precipitation in alloy 718: a combined AEM and APFIM investigation. Superalloys **718**(625), 337–350 (1991). https://doi.org/10.7449/1991/superalloys_1991_337_350
60. K.R. Vishwakarma, N.L. Richards, M.C. Chaturvedi, Microstructural analysis of fusion and heat affected zones in electron beam welded ALLVAC®718PLUS™ superalloy. Mater. Sci. Eng. A **480**, 517–528 (2008). https://doi.org/10.1016/j.msea.2007.08.002
61. X.L. Pan, H.Y. Yu, G.F. Tu, W.R. Sun, Z.Q. Hu, Segregation and diffusion behavior of niobium in a highly alloyed nickel-base superalloy. Trans. Nonferrous Met. Soc. China **21**, 2402–2407 (2011). https://doi.org/10.1016/s1003-6326(11)61027-3
62. C.R. Brundle, C.A. Evans, S. Wilson, *Encyclopedia of materials characterization: surfaces, interfaces, thin films* (Butterworth-Heinemann, Oxford, 1992)
63. R.C. Reed, *The Superalloys, Foundamentals and Applications* (Cambridge University Press, Cambridge, 2006). https://doi.org/10.1017/cbo9781107415324.004
64. J.F. Uginet, B. Pieraggi, Study of secondary grain growth on 718 Alloy. Superalloys **718**, 625–706 (1997). https://doi.org/10.7449/1997/superalloys_1997_343_352
65. R. Watson, M. Preuss, J.Q. da Fonseca, T. Witulski, G. Terlinde, M. Büscher, Characterization of abnormal grain coarsening in Alloy 718. MATEC Web Conf. **14**, 07004 (2014). https://doi.org/10.1051/matecconf/20141407004
66. A. Rollett, F. Humphreys, G.S. Rohrer, M. Hatherly, Recrystallization and Related Annealing Phenomena, 2nd edn, in *Recrystallization and Related Annealing Phenomena*, 2nd edn. (2004) pp. 1–628. https://doi.org/10.1016/b978-0-08-044164-1.x5000-2
67. J.R. Groh, Effect of Cooling Rate From Solution Heat Treatment on Waspaloy Microstructure and Properties, in *Superalloys 1996* (Eighth Int. Symp., 1996) 621–626. https://doi.org/10.7449/1996/superalloys_1996_621_626
68. A. Devaux, A. Helstroffer, J. Cormier, P. Villechaise, J. Douin, M. Hantcherli, F. Pettinari-Sturmel, Effect of aging heat-treatment on mechanical properties of AD730™ superalloy, in *8th Int. Symp. Superalloy 718 Deriv.* (2014) 521–535. https://doi.org/10.1002/9781119016854.ch41
69. L. Whitmore, H. Leitner, E. Povoden-Karadeniz, R. Radis, M. Stockinger, Transmission electron microscopy of single and double aged 718Plus superalloy. Mater. Sci. Eng. A **534**, 413–423 (2012). https://doi.org/10.1016/j.msea.2011.11.089
70. D.A. Porter, K.E. Easterling, *Phase Transformations in Metals and Alloys*, 3rd edn. (CRC Press, Boca Raton, 2009). https://doi.org/10.1201/9781439883570